Article

Miniaturized Piezo Force Sensor for a Medical Catheter and Implantable Device

Bruno Gil,* Bing Li,* Anzhu Gao, and Guang-Zhong Yang

Cite This: *ACS Appl. Electron. Mater.* 2020, 2, 2669–2677

Read Online

ACCESS | 📊 Metrics & More | 📄 Article Recommendations | 🆘 Supporting Information

ABSTRACT: Real-time monitoring of intrabody pressures can benefit from the use of miniaturized force sensors during surgical interventions or for the recovery period thereafter. Herein, we present a force sensor made of poly(vinylidene fluoride)-*co*-trifluoroethylene (P(VDF-TrFE)) with a simple fabrication process that has been integrated into the tip of a medical catheter for intraluminal pressure monitoring, as well as into an implantable device with a power consumption of 180 μW obtained by the near-field communication (NFC) interface to monitor the arterial pulse at the subcutaneous level ($\leq$1 cm). The pressure range supported by the sensor is below 40 kPa, with a signal responsivity of 0.63 μV/Pa and a mean lifetime expectancy of 400 000 loading cycles inside physiological conditions (12 kPa). The proposed sensor has been tested experimentally with synthetic anatomical models for the lungs (bronchoscopy) and subcutaneous tissue, as well as directly above the human carotid and radial arteries. Information about these pressure levels can provide insights about tissue homeostasis inside the body as fluid dynamics are altered in some health conditions affecting the hemodynamic and endocrine body systems, whereas for surgical interventions, precise control and estimation of the pressure exerted by a catheter over the internal walls are necessary to avoid endothelium injuries that lead to bleeding, liquid extravasation, or flow alteration associated with atheroma formation.

KEYWORDS: piezo sensor, medical catheter, implantable device, energy harvesting, intrabody pressure monitoring

Force Sensor   Medical Catheter   Implantable Device
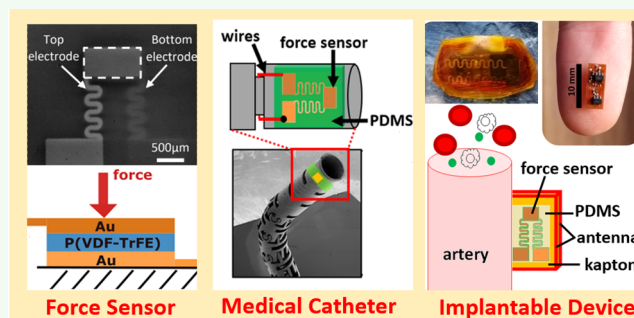
1. INTRODUCTION

Design of miniaturized pressure sensors for medical applications involves a series of fabrication, integration, and biocompatibility issues faced by academics and industries these days. The need for producing small-sized sensors for intrabody pressure monitoring, either by tethered (e.g., catheter)[1] or untethered (implant) solutions[2] requires the use of materials with higher sensitivity to biological tissue loading, higher mechanical stability, and flexibility to navigate the physiological environment or conform to the natural contours of the biological tissues, cavities, and circulating fluids.[3] Materials with a different electrical response to loads, such as piezoelectric, piezoresistive, and capacitive materials, have been integrated into sensors and deployed to respond to these demands. This is found not only for intrabody fluidic pressure monitoring but also on e-skin applications,[4–7] orthopedics,[8,9] drug delivery,[10] tissue growth, and healing.[11]

Piezoresistive sensors have simpler structures than capacitive ones, therefore easier to produce high sensitivity at low pressure values (<5 kPa).[12] Capacitive sensors usually involve a dielectric material sandwiched between conductive electrodes, achieving good sensitivity to high pressures, low hysteresis response, and superior stability.[13,14] Micro or nanostructured patterns fabricated on the elastomer and/or dielectric material,

such as poly(dimethylsiloxane) (PDMS), further enhance the pressure sensing capability of the assembled device.[15] In fact, the increase of the contact area and anchorage points provided by these patterns in the form of pyramids,[16] rugged and spongy structures, leaf structures (bio-mimicking), and hemispheres can help solving adhesion issues to other materials during the fabrication process.[17,18] By its turn, the low permittivity value of PDMS can be tackled by three-dimensional (3D) conductive materials mixed with the elastomer and doped with nanoparticles (like Au, Ag, and Cu) or new composite materials (e.g., graphene,[3,17,19] carbon nanotubes,[1,6] carbon black and polymers,[20] ferromagnetics[8]), therefore contributing to the exploration of new functional principles that lead to increased sensitivities and detection ranges for pressure. Nonetheless, the more complicated the assembled sensor or device is, the more intense, difficult, and costly is the associated fabrication process. The use of nontraditional materials in
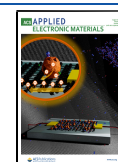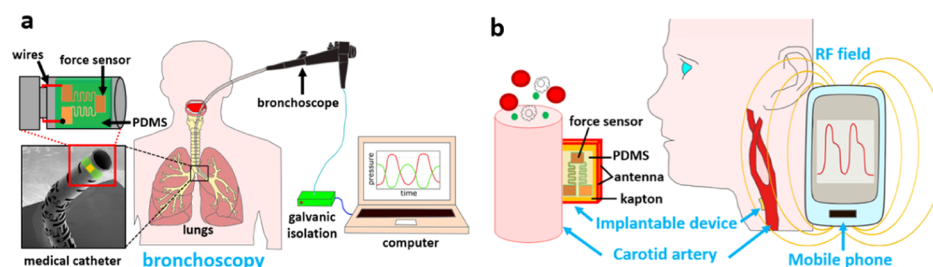
Figure 1. (a) Contextualization images exhibiting a bronchoscopy procedure performed by the proposed medical catheter with attached force sensor and electronic interface to the recording computer. (b) Implantable device placed near the carotid artery, with power harvesting and data transmission capabilities provided by an external mobile phone for future e-health pressure monitoring.

medical products, fabricated by novel methods (such as extrusion printing[21] and fiber weaving[22−24]) or existing ones (lithography, duplicating, and laser microengineering), are neither cost effective nor scalable to achieve in sequence, therefore leading both to the lack of controllability and uniformity distribution of the developed structures within the elastomer, and requiring additional postprocessing techniques such as etching or patterning.[20]

Piezoelectric materials such as poly(vinylidene fluoride) (PVDF)[25] and aluminum nitride (AIN)[26] have lower Young modulus than the more traditional brittle composites made of lead zirconate titanate (PZT) for ultrasound applications, making them easier to fabricate and integrate into flexible substrates, with higher mechanical stretchability and conformity to body geometry. Small, compact, and thin pressure sensors can be fabricated by sandwiching piezoelectric materials between metallic electrodes, as performed in the current study. Sensitivity can still be improved using copolymers or derivatives, such as poly(vinylidene fluoride)-*co*-trifluoroethylene—P(VDF-TrFE)—that combines the piezoelectric effect with ferromagnetic behavior.[4] P(VDF-TrFE) is prepared from solutions (or inks) by printing/casting processes using PVDF in soluble polar solvents, which contribute to a good mechanical and chemical stability for the copolymer. On the other hand, PVDF needs to be stretched to be in the β-phase to yield better piezoelectric characteristics, whereas P(VDF-TrFE) directly crystallizes in a β-like phase, where the chains are in the all-trans conformation. Since PVDF is stretched, it loses its piezoelectric properties above 80 °C due to chain relaxation, while P(VDF-TrFE) can be used up to the Curie temperature during operation, that is, 100 and 135 °C for molar ratios of 70:30 and 80:20, respectively. In addition, this copolymer shows higher crystallinity after annealing and, depending on the polling, better d_{33} coeficient.[27]

The piezoelectric effect can be further explored to develop self-powered implantable devices other than yielding pressure sensing units only. The physiological environment provides the required source of energy, as demonstrated by Zhang et al. with a flexible PVDF film wrapped around the aorta of a porcine, which harvested a total electrical power of 30 nW.[28] However, the intermittent (or noncontinuous) operation of the device is not enough to produce reliable sensing data and transmit it to the exterior of the body due to the general low-frequency content of body movements and/or circulating fluids (<5 Hz). Combination with triboelectric[29] or magnetic materials[30] offers the possibility to increase the harvested power per device area to the order of hundreds μW/cm^2 and harvested voltages above a couple of volts. This may be

sufficient to power up tiny electronically activated implants with rudimentary signal acquisition and conditioning modules, while data transmission is achieved by changing the backscattering properties of the incident energy-carrying magnetic, ultrasonic, or radiofrequency (RF) wave.

Implantable devices are the ideal substitutes for the traditional medical equipment in the forthcoming future, by performing sensing and/or actuation directly over the target tissues,[31−33] without the inconvenient degradation of the signal-to-noise ratio (SNR) of biosignals traveling from internal body sources to off-body detectors. Topics such as device dimension, location, power source (e.g., chemical, piezoelectricity, RF, ultrasounds), sensing modalities (biopotential, temperature, pH, impedance, and pressure), packaging and biocompatibility,[34] permanency or bioresorbability[10,35,36] have occupied researchers lately in the quest of developing implantable devices with adequate sensing accuracy, viable data transmission processes, and safe operation within the body. For pressure monitoring, in particular, direct information about the levels of body fluids can provide insights about tissue homeostasis in the physiological or pathological states, as well as assessing indirectly the supply level of oxygen and other metabolites to the affected body areas.[37]

In this paper, we present a small miniaturized force sensor based on P(VDF-TrFE) with an easy fabrication process and integration into the tip of a medical catheter involved in surgical procedures, to give information about the contact force applied to the intraluminal spaces, as shown in Figure 1a. Moreover, the incorporation of two force sensors disposed laterally on opposite sides of the same catheter allows bilateral pressure sensing during steerable navigation through the physiological environment. Finally, we also embedded a force sensor with an NFC-powered implantable device that is capable of detecting intrabody pressures for distances implant-mobile phone up to 1 cm. This system can be used for arterial pulse detection as NFC signals can cross subcutaneous tissue relatively unscathed (Figure 1b).

2. EXPERIMENTAL SECTION

2.1. Reagent and Apparatus. P(VDF-TrFE) with a 70:30 molar ratio was purchased from Piezotech (France) and all other chemicals in this study were purchased from Sigma-Aldrich (U.K.). A scanning electron microscope (SEM) (Tescan LYRA3) was used to image the bespoke metal catheter (10 kV) and miniaturized sensors (1 kV).

2.2. Procedure for Fabrication of the Force Sensor. P(VDF-TrFE) was dissolved in dimethylformamide (DMF) at a concentration of 1%. The solution was spin-coated onto an atomic-flat highly conductive Si substrate with a speed of 2000 rpm for 30 s and dried at room temperature. The film was annealed at 140 °C for 10 min to improve the overall crystallinity and then poled electrically at 23 °C under AC voltage of increasing amplitude, as described in ref 38.
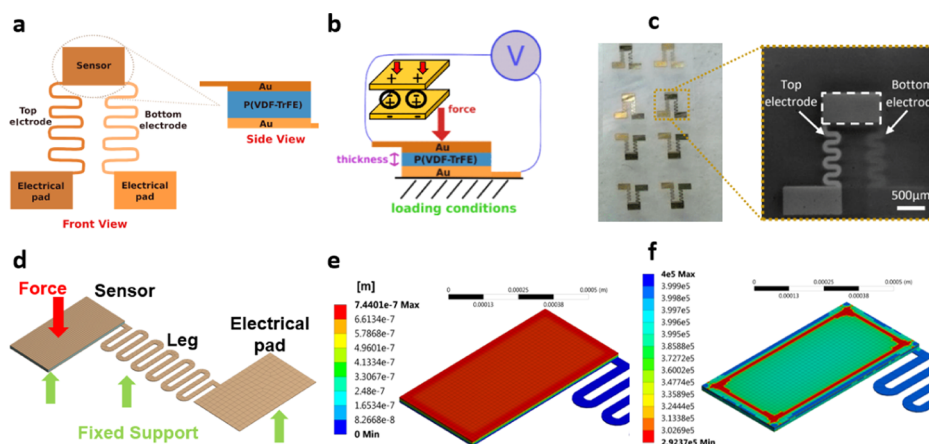
Figure 2. (a) Model of the proposed force sensor, consisting of a central sensing unit made of a layer of piezo film "sandwiched" by two gold electrodes (side view), which connect to the electrical pads (front view). (b) Working principle of the force sensor when actuated by a force applied on the top electrode and mechanically supported by the bottom one, thus inducing an equivalent output voltage (V). (c) Batch of force sensors fabricated on the same piezo film substrate before individually diced (left) and SEM image of an individual force sensor (right). (d) Computational mesh designed for mechanical simulation of the proposed force sensor, with the axial application of the force at the center of the sensing area and fixed support along the bottom surface of the entire structure. (e) Displacement of the sensor for a 10 mN load. (f) Minimum life cycle allocated to the sensor when subjected to a force of 10 mN (fatigue analysis).
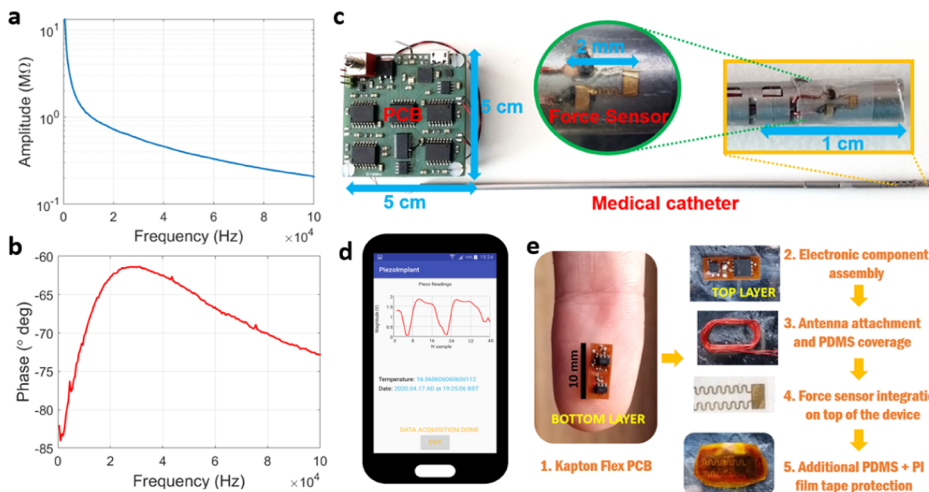

Figure 3. (a) Impedance amplitude variation with frequency for the unloaded force sensor, as measured by a commercial impedance analyzer. (b) Impedance phase variation with frequency for the unloaded sensor. (c) Developed pressure measurement system consisting of the interface PCB connected to the medical catheter, with two force sensors placed on the tip (inlay images show a zoomed view of a sensor). (d) Mobile phone's *app* developed to power and receive the signals produced by the implantable device with an embedded force sensor. (e) Different steps involved in the fabrication of the implantable device with flex PCB design and electronic component assembly, followed by NFC antenna and force sensor integration and final protection by PDMS and PI tape.

Shadow masks were fabricated using a four-axis laser Rofin LFS cutting system (Germany) on the 100 μm thick stainless-steel foil with a cutting resolution of 5 μm. Thermal evaporated Cr with a thickness of 2−3 nm was chosen as an adhesion layer. Sixty nanometer Au film was then evaporated with a slow deposition rate of 2 A/s on top of Cr to achieve a smooth electrode surface. The final structure of a single force sensor is depicted in Figure 2a,b (working principle), as well as on the production batch in Figure 2c, which includes several sensors fabricated on the same film, before individually diced using a scalpel (SEM image).

2.3. Mechanical Characterization of the Force Sensor by Computational Simulation. A 3D model of the entire structure composing the force sensor was designed in ANSYS Mechanical (Ansys Inc., Canonsburg, PA) to analyze the mechanical response of the structure to single and repetitive (fatigue) loading conditions. The structure itself was designed with three different geometrical bodies (solids) corresponding to the bottom Au electrode, piezo film (sensor), and top Au electrode, as shown in Figure 2d. Only the

bottom electrode was modeled as a complete structure, stretching from the center of the film toward the electrical pad (or "leg"), since it mechanically holds the entire structure with fixed supports applied along the bottom surface. By its turn, the top electrode was not modeled with the electrical leg, as it neither contributes to the mechanical analysis nor provides any fixation point to the structure, being free to move toward the bottom electrode according to the loading conditions. Forces were axially applied at the geometrical center of the top electrode, forcing the 20 μm thick film underneath to be compressed (displacement). A total of 11 956 elements (31 478 nodes) were used for the creation of the mesh, with material properties allocated to gold[1] (E_{Au} = 77 GPa, ρ_{Au} = 19 300 kg/m^3, ν_{Au} = 0.25) and piezo film[39] ($E_{P(VDF-TrFE)}$ = 1 GPa, $\rho_{P(VDF-TrFE)}$ = 1.8 kg/m^3, $\nu_{P(VDF-TrFE)}$ = 0.25).

Singly applied forces in the range $\in [1, 30]$ and 1 mN step were experimented in the model to obtain the mechanical displacement, stress (equivalent von-Mises) and strain parameters given by the resolution of the computational system of equations governing the
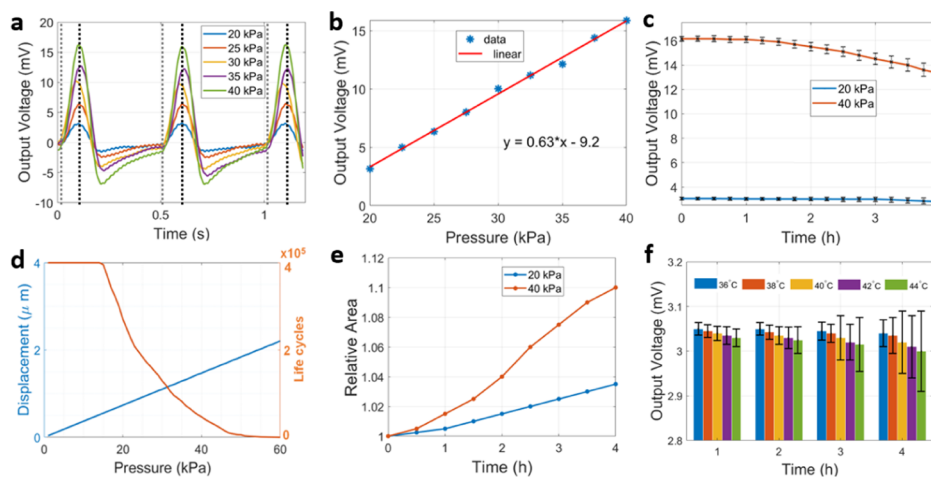
Figure 4. (a) Voltage signals produced by repeated application of different loads (pressure) to the force sensor every 0.5 s, with vertical marks identifying the moment of force contact (dashed gray line) and release (dashed black line). (b) Linear polynomial fit obtained between the applied load and output voltage (maximum value) produced by the force sensor. (c) Evolution of the output voltage (mean value and error bars) for the force sensor during extended repetitive load application with two different intensities (20 and 40 kPa): statistics were calculated in intervals of 15 min during the experiment, with load cycles lasting 0.5 s each. (d) Mechanical simulations showing the evolution of maximum element displacement (in blue) inside the sensor as a function of the applied pressure, as well as the maximum number of life cycles expected for the sensor during fatigue analysis (in orange). (e) Structural evolution of the central sensing area as a function of time, in relation to the original fabricated area (1 mm × 0.5 mm) for two different loads (20 and 40 kPa). (f) Thermal stability analysis in terms of the voltage signal produced by the force sensor for different temperature profiles within the physiological range. Statistics obtained for the mean values and respective error bars were calculated on an hourly basis from measurements taken every 15 min.

isotropic, and elastic regimes. Fatigue analysis was also accomplished by applying loads with constant amplitude to the sensor in reversed cycles, as dictated by the Goodman mean stress theory. The minimum life cycle expected for the sensor was numerically simulated using magnitudes located in the aforementioned interval of forces. Figure 2e shows the displacement of the sensor for a singly applied force (10 mN), whereas Figure 2f depicts the minimum life cycle expected for the different elements composing the sensor subjected to repeated loading by the same force magnitude.

2.4. Procedure for Electrical Characterization of the Force Sensor. The force sensor was connected to copper wires at the electrical pads by conductive electric paint (SKU-0018, Bare Conductive Inc., London, U.K.), before attachment to the input terminals of an impedance analyzer (model E4990A, Keysight Technologies, Santa Rosa, CA). A bipolar electrode configuration was chosen for the measurements, with frequency in the range between DC and 100 kHz, obtaining the curves for amplitude and phase of impedance shown in Figure 3a,b, respectively, and in the condition of mechanical unloading of the sensor. A high value of impedance is registered for the lower spectrum ($\geq$1 MΩ), which is in line with the response of a typical flat piezoelectric transducer, characterized by a strong static or clamped capacitance in the condition of zero loading, whereas phase remains centered at $-90°$, further confirming its capacitive nature.

Since the piezo film exhibited large impedance values at low frequencies, we opted to connect directly the force sensor to an off-the-shelf instrumentation amplifier (IA, INA116, Analog Devices, Norwood, MA) with superior input impedance profile, rather than measuring the sensor response (output) with an oscilloscope probe. The electrical properties of the selected IA—input impedance $\simeq 10^{15}$ Ω and differential input terminals—allowed a direct physical connection with the force sensor, while the guard terminals of IA ensured both noise and electromagnetic interference (EMI) reduction along the signal-carrying wires and all around the force sensor, by connection to a shielded electronic plane made of copper tape (1181-12MM, 3M, Maplewood, MN). The output of the amplifier was then connected to an oscilloscope (MSO-X 3054A, Agilent Technologies, Santa Clara, CA) to record the voltage level produced by the force sensor as a single-ended signal. Though the IA could have provided additional amplification gain to the output signal of the force sensor,

we opted not to amplify it in favor of a one-to-one correspondence between the differential signal generated by the piezo film and the electronically conditioned signal from the IA. Finally, an acoustically activated probe with the associated setup was developed to assist in the application of single or cyclic axial loading to the force sensor, as described in the Supporting Information (Experimental Setup for Cyclic Testing of the Force Sensor section). The adopted conversion between applied voltage signal to the probe and mechanical force (or pressure equivalent) is also presented.

2.5. Design of the Medical Catheter with Attached Force Sensors. Notched metallic tubes with dimensions of OD = 3.33 mm and ID = 2.70 mm were fabricated by the same laser-cutting machine for mask fabrication, as a prototype of a medical catheter. Symmetric slots along the catheter's longitudinal direction were cut in the positions where the sensors were laterally assembled to measure bilateral forces produced in the catheter's external wall by surrounding structures. Two polymer-coated wires were placed along the interior hollow tube of the catheter, with the bottom substrate of each force sensor attached to one wire and the top electrode connected to the other wire. The wires were then linked to the same instrumentation amplifier employed during the electronic characterization of the force sensor but now connected to a fully customized electronic printed circuit board (PCB), for sensor output acquisition, conditioning, isolation and transmission to a computer, as shown in Figure 3c. An additional grounded wire was clipped to the metallic tube of the catheter to reduce both noise and EMI from sources outside the body and manual handling (capacitive coupling). Details of the electronics employed for the interface with the catheter can be found in the Supporting Information (Electronic Design of the Interface for the Medical Catheter section), as well as the performance curves obtained by testing the complete acquisition channel. This interface is battery powered with galvanically isolated communication lines to the computer (recording platform), a requirement for all medical instrumentation interfacing living tissues to avoid a direct physical connection between the power grid lines (computer) and the body (catheter).

In terms of board technology, the PCB was projected in Eagle Cadsoft (Autodesk, Mill Valley, CA) as a double layer rigid board, with a thickness of 1 mm and copper traces for electric signal routing 150 μm wide. Ni/Au surface finishing was selected over the exposed

electrical pads of the PCB, with copper trace protection provided by liquid photoimageable solder mask applied to the top and bottom sides. The off-the-shelf components populating the PCB were then soldered by lead-free solder at a temperature of 330 °C.

2.6. Design of the Implantable Device with Embedded Force Sensor. A small-form and implantable device with planar dimensions of 10 mm × 4 mm was also projected in Eagle to interface a single force sensor for the detection of intrabody pressures, through untethered powering and telemetric links established outside the body. An NFC harvesting module was included on the electronics to generate enough energy from the RF field of a mobile phone, running the *app* developed in Android Studio (Google, Mountain Vale, CA) for pressure signal visualization (Figure 3d). A 30-turns loop antenna made of 0.5 mm thick copper wire (and wrapped around the external perimeter of the device) is responsible for producing a voltage equivalent from the RF field by magnetic induction,[40] followed by rectification of AC signals to deliver a filtered DC voltage to the electronic components embedded on the implant. These components are fully described in the Supporting Information (Electronic Design of the Implantable Device and Pressure Measurement Principle section), together with the mathematical formulas involved in the estimation of the magnitude for the sensed pressure (discrete Fourier transform) and calibration. Impedance measurements at 1 kHz were chosen instead of differential voltage measurements at the terminals of the sensor, as performed previously for the medical catheter (and close to DC) due to the high-power consumption levels of typical IAs and a large occupied area within the circuit board, both incompatible parameters in face of restrictions imposed to implantable devices.

In terms of circuit board design, the implantable device was fabricated on a flexible substrate made of 50 μm thick Kapton material, with electroless deposition of copper traces (35 μm height, 100 μm width) for electric signal routing. A 40 μm thick photoimageable coverlay made of soft epoxy acrylic resin was deposited on top of the copper conductor for thermal and electric signal protection, making the total thickness of the bendable substrate close to 120 μm. A metallization surface finishing for the exposed electrical pads was also performed with silver bath immersion to facilitate posterior component soldering at 330 °C. Electronic components were assembled in the top and bottom layers of the flexible substrate and covered by biocompatible PDMS material, after attachment of the external antenna and solderable enamel wires (0.15 μm diameter) connected to the force sensor (see Figure 3e). The force sensor was then attached to the PMDS-covered layer on the bottom side of the implantable device, with wiring contacts made of silver conductive adhesive epoxy (8331-A, MG Chemicals Ltd., Surrey, BC, Canada). The entire structure was covered again by a thinner layer of PDMS ($\approx$1 mm) for fixation of the sensor to the implantable device, thus providing additional stability and protection when deployed inside the body or other structures. Finally, polyimide film tape (PI, model 1205-1, 3M, Saint Paul, MN) was additionally employed to facilitate adhesion of the device during experimentation to synthetic phantoms or the human skin.

3. RESULTS AND DISCUSSION

3.1. Mechanical Testing of the Single Force Sensor by Experimentation and Computational Simulations. The mechanical response of the sensor to axial loading is shown in Figure 4a, using different pressure intensities that reach the central area of the sensor as imposed by the acoustically activated probe. The range of pressure values tested was below 40 kPa and within the physiological limits found inside biological tissues, cavities or circulating fluids. Repetitive application of the load every 0.5 s allowed to measure consistently the output voltage produced by the force sensor due to the mechano-piezoelectric coupling effect. A linear relationship was established between the peak output voltage of the sensor and the intensity of pressure, as shown in Figure 4b, from where the signal responsivity could be estimated at a

level of 0.63 μV/Pa. Additional stability analysis was performed by applying a repetitive load (every 0.5 s, with intensities of 20 and 40 kPa) for longer periods of time (4 h or, equivalently, 28 800 loading cycles) while recording the voltage level generated by the force sensor. The temporal evolution of the voltage levels for these loads is shown in Figure 4c, as the statistical mean (and respective standard deviation) calculated over temporal intervals of 15 min. These results show a steady output voltage (on average) produced by the force sensor (ΔV = 0.25 mV) at intensities of 20 kPa and decreasing output voltage over time with levels of 40 kPa (ΔV = 2.85 mV).

In terms of the mechanical simulations, Figure 4d shows the displacement produced on the piezo film subjected to different pressures, obtaining a linear displacement of the sensor to axial loading in the range from 0 to 30 mN (or, equivalently, 0−60 kPa), at a rate of 38 μm/Pa (blue signal), with a maximum displacement of 2.25 μm recorded at the higher pressure level. Fatigue analysis of the structure in the condition of cyclic loading with different magnitudes (orange signal) has revealed a life cycle expectancy characterized by two plateau zones in the low- and higher-pressure range, respectively, and interleaved by a middle zone where the number of life cycles is highly dependent on pressure, with a quadratic negative coefficient. The simulated life cycle for the force sensor has shown a complete collapse of its structure above 45 kPa and a stable response for pressures below 15 kPa. By considering a mean arterial pressure of 87.5 mmHg ($\approx$12 kPa) in physiological conditions, this translates into a mean life of 400 000 pressure cycles for the force sensor, corresponding, in turn, to a continuous operation for 320 000 s ($\approx$90 h), this considering also the average duration for the cardiac cycle and heart rate expected in healthy individuals (75 beats per minute).[1,41]

Additionally, we performed more experimental tests to investigate the modification of the sensor's structure by taking microscopic images of several sensors subjected to the same loading conditions as before (20 and 40 kPa) but for different temporal extensions (loading cycles). We investigated only the geometrical change in the central sensing area relative to the original "unloaded" area. Figure 4e shows the evolution of the change in the central area by concatenating together measurements taken from different sensors over time. From the obtained curves, a load of 20 kPa produces a linear increment on the central area ($\Delta A/\Delta t$) at a rate of 3750 μm^2/ h, whereas for the 40 kPa load, the curve exhibit a semiquadratic behavior with a maximum variation of 10% after 4 h of repetitive loading cycles.

Finally, thermal stability analysis of the force sensor was also estimated by measuring the voltage output in the condition of varying temperatures within the physiological range (<45 °C), as intended for sensor applications inside the human body. A hotplate (442-0662, VWR International, Radnor, PA) was placed below the force sensor, thus replacing the force-sensing platform (scale) while keeping the same actuation setup to deliver an axial load of 20 kPa. The evolution of the voltage levels produced by the sensor subjected to different temperature profiles is shown in Figure 4f, as an hourly average calculated for measurements taken every 15 min. The obtained results reveal a decline of the sensor output (in average) for temperatures above 40 °C, while the uncertainty in voltage measurements (error bars) increases at a higher rate for the last hours of the experiment but still confined within $\approx$6.7% of the average voltage produced by the sensor for 20 kPa loads.
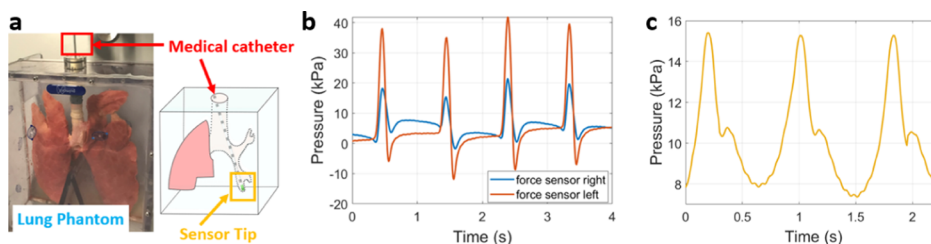
Figure 5. (a) Lung phantom employed to test the medical catheter with bilateral pressure sensing (contact). (b) Simultaneous pressure signals obtained by the two force sensors inside the left lobar branch of the lung. (c) Pressure signals detected by the medical catheter (single sensor) in contact with the surface of the skin and above the right carotid artery (neck).
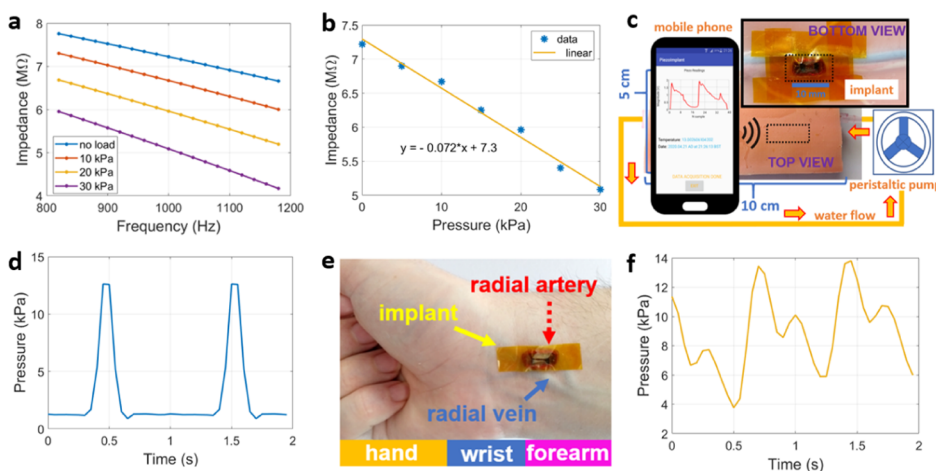

Figure 6. (a) Impedance amplitude variation of the force sensor when actuated by different loads and centered around 1 kHz measured by a commercial impedance analyzer. (b) Linear fit relating impedance variation of the sensor with the applied load at 1 kHz. (c) Experimental setup developed for pressure monitoring by means of an anatomical phantom of the skin and subcutaneous tissues, with a circulation of water through the synthetic artery and implantable device placed on its walls (bottom view); the latter receiving the RF power from the opposite side of the phantom (top view). (d) Water pressure signal detected by the implantable device. (e) Location of the implantable device over the radial arterial (wrist). (f) Radial pressure signal displayed by the NFC-enabled mobile phone.

3.2. Integration of the Force Sensors with the Medical Catheter. With the complete mechanical characterization of the force sensor, we proceeded to the integration of two sensors into the tip of a medical catheter. The sensors were placed on different sides along the external contour of the catheter and connected to the developed medical catheter interface. Experiments with this system were carried out using a synthetic phantom of the lungs (Figure 5a), with the catheter navigating through the trachea, left bronchi, and reaching the ramifications of the lobar branches until physical contact with their walls was established. Contact pressure signals recorded by repeatedly and gently moving back and forth the catheter through this narrow air passage are depicted in Figure 5b. Measurement of the human arterial pulse was also performed by placing the tip of the catheter (one side only) in contact with the skin surface above the carotid artery on the right side of the body neck, thus obtaining the pressure signal shown in Figure 5c.

The high linearity level achieved by the amplification channel in the interface electronics relative to input signals with magnitudes below 20 mV (see Figure S3b with $\Delta V \approx 1.6$ V) and frequency ≤ 100 Hz (Figure S3c: $\Delta V \approx 0.2$ V) contributed both to a good matching with the voltages generated by the fabricated force sensor, important for achieving a satisfactory tracking of the pressure waveforms derived either from the body (arterial pulse) or mechanical actuation (acoustically activated probe). By its turn, the

extremely high-input impedance of the instrumentation amplifiers on the interface electronics allowed a direct physical connection to the sensor without significant signal degradation in the lower frequency range. The employed IAs also contributed for the permanency of the electric charges within the piezo film of the sensor, thus allowing electrical currents to circulate in-between in the femtoampere range only.

3.3. Force Sensor Attached to the Implantable Device. On the contrary, the extremely high impedance presented by the force sensor close to DC had a negative impact on the availability of small-form electronic components to be embedded on the implant side, and without exhausting the harvested power level. The solution found in this study to overcome this issue was to stimulate the force sensor at 1 kHz, where the impedance levels of the sensor were slightly lower than DC, as shown in Figure 6a for different loading conditions at 1 kHz. The corresponding linear fit in Figure 6b presents a negative coefficient of 71 Ω/Pa. The implantable device with the attached force sensor was first tested in a synthetic anatomical phantom (Figure 6c), composed of a polyurethane tube mimicking an artery vessel with circulating water flow imposed by a peristaltic pump (REGLO ICC, Ismatec, Wertheim, Germany) at controllable speeds. An example of the pressure signal captured by the mobile phone placed on the opposite side of the phantom (0.5 cm gap) is shown in Figure 6d, where the pressure variations due to the pulsatile flow of water are clearly visible (signal peaks), whose duration in time

is dictated by the flow velocity. During the second set of experiments, the implant was pressed against the skin on the wrist of volunteers to detect the pulse signal directly above the radial artery (Figure 6e), thus obtaining a signal waveform of the form exhibited in Figure 6f. Although the update rate for the impedance estimation inside the implantable device was only 50 ms due to limited resources on the embedded electronics, it is still enough to discriminate important temporal features occurring inside the arterial pulse such as the dicrotic notch, and within physiological limits (amplitude).

Regarding the harvested voltage levels (see Figure S4c), the proposed implantable device could be powered up to full operation at a maximum distance of 1 cm from the mobile phone. The measured curve exhibited a quadratic decreasing profile from a maximum value of 2.6 V (zero gap) to a minimum of 0.5 V (gap of 1.5 cm). Though this curve was obtained in open-air conditions (and alignment between antennas), small variations to the harvested levels would have likewise been obtained inside tissues since the magnetic permeability contrast between them and air is negligible.[42] Regarding the calculation of the amplitude for impedance at 1 kHz, results obtained from Figure S4b reveal lower estimates by the implantable device as compared to calibrated resistors. This discrepancy is more pronounced at extremes of impedance (1 and 10 MΩ), with an average 2% decrease in the estimated impedance values given by the linear fit obtained.

Finally, the proposed sensor and associated systems do not come without their drawbacks. Biocompatibility on the longer term requires thicker layers of PDMS (or additional materials such as Parylene) that inevitably damp the response of the sensor to mechanical loading. Investment on more biocompatibility studies is necessary for the future not only to evaluate in the long-term the behavior of these extra layers inside a saline physiological environment but also to establish the biocompatibility of other pressure-sensitive materials (such as PVDF only) or composites directly in contact with the internal body tissues. Moreover, the voltage levels produced by the actual force sensor are still 2 orders of magnitude lower than the level required to sustainably power up the embedded electronics on the implant side,[34] hence the need to rely on external NFC links (active device). For passive devices, the pressure level is directly coded on the backscattered signal of the transmitting energy wave (shift in resonance frequency), though highly dependent on the distance implant-external source that decreases drastically the sensitivity and range for the detection of intrabody pressures. Additional parameters such as the internal body temperature could have also been monitored since the proposed implantable device possesses an indicator for this parameter, although temperature variations induced by pressure gradients were already outside the scope of the present study, as well as the use of more force sensors working simultaneously on the tip of the catheter to increase the spatial resolution for the recorded pressure in highly irregular domains such as the body tissues. These two approaches are left in here as future work. Nonetheless, the proposed force sensor presents some advantages in comparison to other publications with film-type polymer-based materials employed in larger sensing areas such as human hand or feet[12,43] (achieving sensitivities of 40 mN only), or micro-electromechanical system (MEMS) pressure devices, which involve complex processes for fabrication, deposition, and integration of piezo elements that lower the original simulated pressure range.[44]

4. CONCLUSIONS

This work presents a force sensor made of P(VDF-TrFE) as the piezo sensing layer, with medical application in the monitoring of body pressures by integration into the tip of a medical catheter and implantable device. Precise control and estimation of the force (or pressure) exerted by the catheter over the internal walls of vessels and intrabody cavities is of vital importance during surgical intervention since an injured endothelium can then lead to bleeding or liquid extravasation between separated spaces inside the body or, worse, alteration to blood flow (shear stress) involved in atheroma formation. By its turn, small-form implantable pressure devices can be left at the surgical site to monitor the redistribution of body fluids during the recovery period thereafter. Reposition of the physiological pressure levels verified before surgery is essential to achieve proper tissue healing. Failure to do so can create a spot for fluidic disturbance or retention, with potential hazards for bacterial invasion and colonization, as often found in medical-surgical site infections. Other pathological conditions affecting the hemodynamic and endocrine body systems can also have repercussions on the dynamics and distribution of internal fluids that are susceptible to be monitored by the pressure-sensitive implantable device described in the current manuscript.

■ ASSOCIATED CONTENT

ⓈI Supporting Information

The Supporting Information is available free of charge at https://pubs.acs.org/doi/10.1021/acsaelm.0c00538.

> Description of the experimental setup developed to test mechanically the force sensor; details about the electronics inside the medical catheter interface and implantable device for sensor signal acquisition; and the pressure measuring principle followed by the latter system (PDF)

■ AUTHOR INFORMATION

Corresponding Authors

Bruno Gil − *The Hamlyn Centre, Imperial College London, London SW7 2AZ, U.K.;* ⓞ orcid.org/0000-0001-8054-059X; Phone: +44(0)7470311442; Email: b.gil-rosa@imperial.ac.uk

Bing Li − *The UK DRI Care Research and Technology Centre, Department of Brain Science, Imperial College London, London W12 0NN, U.K.;* ⓞ orcid.org/0000-0002-1737-3423; Phone: +44(0)79358668643; Email: b.li@imperial.ac.uk

Authors

Anzhu Gao − *Institute of Medical Robotics, Shanghai Jiao Tong University, Shanghai 200240, China*

Guang-Zhong Yang − *Institute of Medical Robotics, Shanghai Jiao Tong University, Shanghai 200240, China*

Complete contact information is available at:
https://pubs.acs.org/10.1021/acsaelm.0c00538

Author Contributions

The manuscript was written through the contributions of all authors. All authors have given approval to the final version of the manuscript. B.G. and B.L. developed the interface electronics for the medical catheter and implantable device and designed the force sensor, respectively. A.G. developed the medical catheter. G.-Z.Y. supervised the work.

ABBREVIATIONS

AC, alternating current; AIN, aluminum nitride; DC, direct current; DMF, dimethylformamide; EMI, electromagnetic interference; FR-4, grade of epoxy laminated material; IA, instrumentation amplifier; ID, inner diameter; MEMS, micro-electromechanical system; NFC, near-field communication; OD, outer diameter; PDMS, poly(dimethylsiloxane); PI, polyimide; PVDF, poly(vinylidene); P(VDF-TrFE), poly-(vinylidene fluoride)-*co*-trifluoroethylene; PZT, zirconate titanate; RF, radio frequency; SEM, scanning electron microscope; SNR, signal-to-noise ratio

REFERENCES

(1) Li, B.; Gil, B.; Power, M.; Gao, A.; Treratanakulchai, S.; Anastasova, S.; Yang, G.-Z. Carbon-Nanotube-Coated 3D Micro-spring Force Sensor for Medical Applications. *ACS Appl. Mater. Interfaces* **2019**, *11*, 35577−35586.

(2) Lee, J. O.; Park, H.; Du, J.; Balakrishna, A.; Chen, O.; Sretavan, D.; Choo, H. A microscale optical implant for continuous in vivo monitoring of intraocular pressure. *Microsyst. Nanoeng.* **2017**, *3*, No. 17057.

(3) Lou, Z.; Chen, S.; Wang, L.; Jiang, K.; Shen, G. An ultra-sensitive and rapid response speed graphene pressure sensors for electronic skin and health monitoring. *Nano Energy* **2016**, *23*, 7−14.

(4) Yoon, S.; Sim, J. K.; Cho, Y.-H. A flexible and wearable human stress monitoring patch. *Sci. Rep.* **2016**, *6*, No. 23468.

(5) Ge, J.; Wang, X.; Drack, M.; Volkov, O.; Liang, M.; Bermúdez, G. S. C.; Illing, R.; Wang, C.; Zhou, S.; Fassbender, J.; et al. A bimodal soft electronic skin for tactile and touchless interaction in real time. *Nat. Commun.* **2019**, *10*, No. 4405.

(6) Boutry, C. M.; Negre, M.; Jorda, M.; Vardoulis, O.; Chortos, A.; Khatib, O.; Bao, Z. A hierarchically patterned, bioinspired e-skin able to detect the direction of applied pressure for robotics. *Sci. Robot.* **2018**, *3*, No. eaau6914.

(7) Hua, Q.; Sun, J.; Liu, H.; Bao, R.; Yu, R.; Zhai, J.; Pan, C.; Wang, Z. L. Skin-inspired highly stretchable and conformable matrix networks for multifunctional sensing. *Nat. Commun.* **2018**, *9*, No. 244.

(8) Wu, Y.; Liu, Y.; Zhou, Y.; Man, Q.; Hu, C.; Asghar, W.; Li, F.; Yu, Z.; Shang, J.; Liu, G. A skin-inspired tactile sensor for smart prosthetics. *Sci. Robot.* **2018**, *3*, No. eaat0429.

(9) Boutry, C. M.; Kaizawa, Y.; Schroeder, B. C.; Chortos, A.; Legrand, A.; Wang, Z.; Chang, J.; Fox, P.; Bao, Z. A stretchable and biodegradable strain and pressure sensor for orthopaedic application. *Nat. Electron.* **2018**, *1*, 314−321.

(10) Suhardi, V. J.; Bichara, D. A.; Kwok, S. J. J.; Freiberg, A. A.; Rubash, H.; Malchau, H.; Yun, S. H.; Muratoglu, O. K.; Oral, E. A fully functional drug-eluting joint implant. *Nat. Biomed. Eng.* **2017**, *1*, No. 0080.

(11) Shin, J.; Yan, Y.; Bai, W.; Xue, Y.; Gamble, P.; Tian, L.; Kandela, I.; Haney, C. R.; Spees, W.; Lee, Y.; et al. Bioresorbable pressure sensors protected with thermally grown silicon dioxide for the monitoring of chronic diseases and healing processes. *Nat. Biomed. Eng.* **2019**, *3*, 37−46.

(12) Sundaram, S.; Kellnhofer, P.; Li, Y.; Zhu, J.-Y.; Torralba, A.; Matusik, W. Learning the signatures of the human grasp using a scalable tactile glove. *Nature* **2019**, *569*, 698−702.

(13) Kaisti, M.; Panula, T.; Leppänen, J.; Punkkinen, R.; Tadi, M. J.; Vasankari, T.; Jaakkola, S.; Kiviniemi, T.; Airaksinen, J.; Kostiainen, P.; et al. Clinical assessment of a non-invasive wearable MEMS pressure sensor array for monitoring of arterial pulse waveform, heart rate and detection of atrial fibrillation. *npj Digit. Med.* **2019**, *2*, No. 39.

(14) Hwang, B.-U.; Zabeeb, A.; Trung, T. Q.; Wen, L.; Lee, J. D.; Choi, Y.-I.; Lee, H.-B.; Kim, J. H.; Han, J. G.; Lee, N.-E. A transparent stretchable sensor for distinguishable detection of touch and pressure by capacitive and piezoresistive signal transduction. *NPG Asia Mater.* **2019**, *11*, No. 23.

(15) Mahata, C.; Algadi, H.; Lee, J.; Kim, S.; Lee, T. Biomimetic-inspired micro-nano hierarchical structures for capacitive pressure sensor applications. *Measurement* **2020**, *151*, No. 107095.

(16) Jung, M.; Vishwanath, S. K.; Kim, J.; Ko, D.-K.; Park, M.-J.; Lim, S.-C.; Jeon, S. transparent and flexible Mayan-pyramid-based pressure Sensor using facile-transferred indium tin oxide for Bimodal Sensor Applications. *Sci. Rep.* **2019**, *9*, No. 14040.

(17) Kou, H.; Zhang, L.; Tan, Q.; Liu, G.; Dong, H.; Zhang, W.; Xiong, J. Wireless wide-range pressure sensor based on graphene/PDMS sponge for tactile monitoring. *Sci. Rep.* **2019**, *9*, No. 3916.

(18) Liu, C.; Zhu, W.; Li, M.; Sun, X.; Guo, X.; Liu, J.; Liu, P.; Zhang, Y.; Huang, Y. Highly stable pressure sensor based on carbonized melamine sponge using fully wrapped conductive path for flexible electronic skin. *Org. Electron.* **2020**, *76*, No. 105447.

(19) Tian, H.; Shu, Y.; Wang, X.-F.; Mohammad, M. A.; Bie, Z.; Xie, Q.-Y.; Li, C.; Mi, W.-T.; Yang, Y.; Ren, T.-L. A graphene-based resistive pressure sensor with record-high sensitivity in a wide pressure range. *Sci. Rep.* **2015**, *5*, No. 8603.

(20) Pruvost, M.; Smit, W. J.; Monteux, C.; Poulin, P.; Colin, A. Polymeric foams for flexible and highly sensitive low-pressure capacitive sensors. *npj Flexible Electron.* **2019**, *3*, No. 7.

(21) Gao, Y.; Xu, M.; Yu, G.; Tan, J.; Xuan, F. Extrusion printing of carbon nanotube-coated elastomer fiber with microstructures for flexible pressure sensors. *Sens. Actuators, A* **2019**, *299*, No. 111625.

(22) Li, P.; Zhao, L.; Jiang, Z.; Yu, M.; Li, Z.; Zhou, X.; Zhao, Y. A wearable and sensitive graphene-cotton based pressure sensor for human physiological signals monitoring. *Sci. Rep.* **2019**, *9*, No. 14457.

(23) Zhou, Y.; He, J.; Wang, H.; Qi, K.; Nan, N.; You, X.; Shao, W.; Wang, L.; Ding, B.; Cui, S. Highly sensitive, self-powered and wearable electronic skin based on pressure-sensitive nanofiber woven fabric sensor. *Sci. Rep.* **2017**, *7*, No. 12949.

(24) An, B. W.; Heo, S.; Ji, S.; Bien, F.; Park, J.-U. Transparent and flexible fingerprint sensor array with multiplexed detection of tactile pressure and skin temperature. *Nat. Commun.* **2018**, *9*, No. 2458.

(25) Sekine, T.; Sugano, R.; Tashiro, T.; Sato, J.; Takeda, Y.; Matsui, H.; Kumaki, D.; Dos Santos, F. D.; Miyabo, A.; Tokito, S. Fully printed wearable vital sensor for human pulse rate monitoring using ferroelectric polymer. *Sci. Rep.* **2018**, *8*, No. 4442.

(26) Signore, M.; Rescio, G.; De Pascali, C.; Iacovacci, V.; Dario, P.; Leone, A.; Quaranta, F.; Taurino, A.; Siciliano, P.; Francioso, L. Fabrication and characterization of AlN-based flexible piezoelectric pressure sensor integrated into an implantable artificial pancreas. *Sci. Rep.* **2019**, *9*, No. 17130.

(27) Soulestin, T.; Ladmiral, V.; Dos Santos, F. D.; Ameduri, B. Vinylidene fluoride- and trifluoroethylene-containing fluorinated electroactive copolymers. *Prog. Polym. Sci.* **2017**, *72*, 16−60.

(28) Zhang, H.; Zhang, X.-S.; Cheng, X.; Liu, Y.; Han, M.; Xue, X.; Wang, S.; Yang, F.; Smitha, A.; Zhang, H.; et al. A flexible and implantable piezoelectric generator harvesting energy from the pulsation of ascending aorta: in vitro and in vivo studies. *Nano Energy* **2015**, *12*, 296−304.

(29) Jung, W.-S.; Kang, M.-G.; Moon, H. G.; Baek, S.-H.; Yoon, S.-J.; Wang, Z.-L.; Kim, S.-W.; Kang, C.-Y. High output piezo/triboelectric hybrid generator. *Sci. Rep.* **2015**, *5*, No. 9309.

(30) Cheng, L.; Yuan, M.; Gu, L.; Wang, Z.; Qin, Y.; Jing, T.; Wang, Z. L. Wireless, power-free and implantable nanosystem for resistance-based biodetection. *Nano Energy* **2015**, *15*, 598−606.

(31) Zhang, Y.; Mickle, A. D.; Gutruf, P.; McIlvried, L. A.; Guo, H.; Wu, Y.; Golden, J. P.; Xue, Y.; Grajales-Reyes, J. G.; Wang, X.; et al. Battery-free, fully implantable optofluidic cuff system for wireless optogenetic and pharmacological neuromodulation of peripheral nerves. *Sci. Adv.* **2019**, *5*, No. eaaw5296.

(32) Zhang, H.; Gutruf, P.; Meacham, K.; Montana, M. C.; Zhao, X.; Chiarelli, A. M.; Vázquez-Guardado, A.; Norris, A.; Lu, L.; Guo, Q.; et al. Wireless, battery-free optoelectronic systems as subdermal implants for local tissue oximetry. *Sci. Adv.* **2019**, *5*, No. eaaw0873.

(33) Gutruf, P.; Yin, R. T.; Lee, K. B.; Ausra, J.; Brennan, J. A.; Qiao, Y.; Xie, Z.; Peralta, R.; Talarico, O.; Murillo, A.; et al. Wireless, battery-free, fully implantable multimodal and multisite pacemakers for applications in small animal models. *Nat. Commun.* **2019**, *10*, No. 5742.

(34) Yang, G.-Z. *Implantable Sensors and Systems: From Theory to Practice*; Springer, 2018.

(35) Shin, J.; Liu, Z.; Bai, W.; Liu, Y.; Yan, Y.; Xue, Y.; Kandela, I.; Pezhouh, M.; MacEwan, M. R.; Huang, Y.; et al. Bioresorbable optical sensor systems for monitoring of intracranial pressure and temperature. *Sci. Adv.* **2019**, *5*, No. eaaw1899.

(36) Kang, S.-K.; Murphy, R. K.; Hwang, S.-W.; Lee, S. M.; Harburg, D. V.; Krueger, N. A.; Shin, J.; Gamble, P.; Cheng, H.; Yu, S.; et al. Bioresorbable silicon electronic sensors for the brain. *Nature* **2016**, *530*, 71−76.

(37) Vinje, V.; Ringstad, G.; Lindstrøm, E. K.; Valnes, L. M.; Rognes, M. E.; Eide, P. K.; Mardal, K.-A. Respiratory influence on cerebrospinal fluid flow−a computational study based on long-term intracranial pressure measurements. *Sci. Rep.* **2019**, *9*, No. 9732.

(38) Bargain, F.; Panine, P.; Dos Santos, F. D.; Tence-Girault, S. From solvent-cast to annealed and poled poly(VDF-*co*-TrFE) films: New insights on the defective ferroelectric phase. *Polymer* **2016**, *105*, 144−156.

(39) Piezotech. Piezoelectric Films Technical Information, 2015. Available Online at: http://www.piezotech.fr (accessed March 20, 2020).

(40) Rosa, B. M. G.; Anastasova-Ivanova, S.; Yang, G.-Z. NFC-Powered Flexible Chest Patch for Fast Assessment of Cardiac, Hemodynamic and Endocrine Parameters. *IEEE Trans. Biomed. Circuits Syst.* **2019**, *13*, 1603−1614.

(41) Ganong, W. *Review of Medical Physiology*, 24th ed.; McGraw-Hill Education/Medical: New York, 2014.

(42) Grimnes, S.; Martinsen, O. *Bioimpedance and Bioelectricity Basics*, 3rd ed.; Academic Press, 2014.

(43) Sharma, T.; Aroom, K.; Naik, S.; Gill, B.; Zhang, J. X. Flexible thin-film PVDF-TrFE based pressure sensor for smart catheter applications. *Ann. Biomed. Eng.* **2013**, *41*, 744−751.

(44) Park, W. T.; Kotlanka, R. K.; Lou, L.; Humidullah, M.; Lee, C. MEMS tri-axial force sensor with an integrated mechanical stopper for guidewire applications. *Microsyst. Technol.* **2013**, *19*, 1005−1015.